Tellus (2003), 55A, 255–272
Printed in UK. All rights reserved

TELLUS
ISSN 0280–6495

Influence of a step-like coastline on the basin scale vorticity budget of mid-latitude gyre models

By FRÉDÉRIC DUPONT[1,2,3]*, DAVID N. STRAUB[1,2] and CHARLES A. LIN[1,2,3], [1]*Department of Atmospheric and Oceanic Sciences, McGill University, 805 Sherbrooke O, Montréal, QC H3A 2K6, Canada;* [2]*Centre for Climate and Global Change Research (C*^{2}*GCR) 805 Sherbrooke O, Montréal, QC, H3A 2K6, Canada;* [3]*Centre de recherche en calcul appliqué (CERCA) 5160 Décarie, Suite 400, Montréal, QC, H3X 2H9, Canada*

(Manuscript received 12 February 2002; in final form 8 November 2002)

ABSTRACT

Global vorticity budgets in C-grid shallow water (SW) and quasi-geostrophic (QG) models of wind-driven ocean circulation with free-slip boundary conditions are considered. For both models, it is pointed out that the discretized vorticity equation is defined only over a subdomain that excludes boundary grid nodes. At finite resolution, this implies an advective flux of vorticity across the perimeter of the discretized vorticity domain. For rectangular basins where grid axes are aligned with the basin walls, this flux tends to zero as resolution is increased. We also consider the case in which the grid is rotated with respect to the basin, so that a step-like coastline results. Increased resolution then leads to more steps and, because the advective flux of vorticity out of the domain is particularly large at steps, it is no longer obvious that increased resolution should reduce the advective flux. Results are found to be sensitive to numerical details. In particular, we consider different formulations for the non-linear terms (for both the SW and QG models) and two formulations of the viscous stress tensor for the SW model [the conventional five-point Laplacian and the δ–ζ stress tensor suggested by Madec et al. (*J. Phys. Oceanogr*. **21**, 1349–1371)]. For the SW model, the overall circulation and the behavior of the flux term are dependent on both the formulation of the viscous stress tensor and the non-linear terms. The best combination is found to be the δ–ζ tensor with an enstrophy-preserving advection scheme. With this combination, the circulation of the non-rotated basin is recovered in rotated basins and the advective flux tends to converge towards zero with increasing resolution. The poorest combination is the δ–ζ tensor with the conventional advective scheme. In this case, the advective flux term diverges with increasing resolution for some rotation angles and the model crashes for some others. For the QG model, the convergence order of the advective flux term of absolute vorticity is near unity (roughly the same as with the SW model). Most of the error (especially at high resolution) is related to errors in the β term (which is hidden in the advective contribution in the SW model). However, the overall circulation is less sensitive to the rotation of the grid with respect to the basin, especially when the Jacobian proposed by Arakawa (*J. Comput. Phys*. **1**, 119–143) is used.

1. Introduction

Much of the theory of large-scale ocean circulation is based on analytic and numerical calculations carried out in basins having simple, most often rectangular, geometric forms. The motivation for this approach has mainly to do with the added simplicity it offers. Thus, while the introduction of complex forms of actual basins will necessarily lead to large deformations of the circulation, it is hoped that a thorough understanding of the simple geometry problems will translate to at least a qualitative understanding of the actual ocean. Simple basin shapes also offer

*Corresponding author. Current affiliation: Coastal Oceanography, Bedford Institute of Oceanography, PO Box 1006, Dartmouth, NS B2Y-4A2, Canada.
e-mail: dupontf@mar.dfo-mpo.gc.ca

obvious numerical advantages. For example, in finite difference models, horizontal grid axes are generally chosen to correspond with the orientation of (rectangular) basin walls. It was pointed out by Adcroft and Marshall (1998, hereafter referred as AM) that when this orientation is not chosen, numerical problems associated with the artificial steps introduced in the discretized geometery can have an $O(1)$ impact on circulation strength and patterns. This is especially evident under the free-slip dynamic boundary condition. Furthermore, when more realistic geometries are considered, these artificial steps are unavoidable, at least in finite difference formulations, which are often employed in general circulation models. Moreover, modelers typically refine the coastline geometry as resolution increases. Thus, although the steps become smaller, their number increases with increasing resolution. It is then not obvious that numerical problems associated with the steps disappear as resolution is increased. That is, presumably smaller steps pose less of a problem individually; however, that there are more of them poses more of a problem.

Ocean circulation theory also relies heavily on ideas relating to potential vorticity (Gill, 1982; Pedlosky, 1987; 1996) and one is often interested in basin integrated vorticity, or potential vorticity budgets. In fact, "difficulties" in closing the vorticity budget seem to be related to the problem of inertial runaway (Pedlosky, 1996). That is, it is observed in numerical integrations of, for example, the single gyre Munk problem, that velocities become unrealistically large as viscosity is reduced from grossly unrealistic (large) values towards more palatable, smaller ones (Ierley and Sheremet, 1995). The problem is more severe under free slip boundary conditions because the free slip boundary layer is less effective at achieving a vorticity flux across the basin perimeter. One of the points made in the present manuscript is that it is often difficult to define numerically meaningful vorticity budgets, except in a subportion of the model domain that excludes a thin strip adjacent to the wall. Put another way, at least in certain circumstances, there is an artificial source/sink term of vorticity immediately adjacent to the boundary. This numerical artifact is particularly problematic in model geometries having step-like structures in the basin walls. Given that these structures are generic (assuming finite difference methods and complex coastline forms), this may lead to problems in accurately calculating vorticity budgets, which may otherwise be useful in analyzing output from general circulation models (e.g., Wells and de Cuevas, 1995).

This problem is made even more dramatic by the fact that all the terms in the vorticity budget can be recast into boundary integrals. This suggests that values of these integrals may be sensitive to coastline representation in the model. Because we discard a thin strip along the model boundary for computing vorticity budgets, we allow for an advective flux of vorticity through the lateral boudaries (to be explained later). This term is usually small and decreases with increasing resolution in rectangular geometries. However, the advective flux of vorticity is particularly large at steps, and it is no longer obvious that increased resolution should reduce this term. We are therefore concerned about the numerical formulation of the advective terms in numerical models of the ocean and how it affects the vorticity budget calculation (and by extension the overall circulation). As did AM, we also expect to find sensitivity to the formulation of the viscous dissipation terms. They considered only one advection scheme, and found a marked improvement when the viscous terms were represented as in Madec et al. (1991). Here, we hope to find an optimal combination of the two that will minimize the influence of artificial steps.

The details of the discretization may vary depending on the staggering of the different variables on the grid. Typically, in the more general context of the primitive equations, the equations are solved on a structured grid using one of several standard staggering techniques: the A-grid (Dietrich et al., 1993), B-grid (Bryan, 1969; Cox, 1984) or C-grid (Bleck and Boudra, 1981; Blumberg and Mellor, 1983). Structured grids facilitate employment of second or higher order accuracy for the discretized equations, but make awkward accurate representation of boundaries. More precisely, where the orientation of the boundary does not correspond to that of the grid, discretization of the boundary introduces a series of artificial 'steps' along the coast (Fig. 1). For example, three-dimensional z-coordinate models have meridional circulations which are known to be sensitive to the details of how the bottom boundary is represented. More precisely, the issue is that they do not accurately advect denser waters along slopes and overestimate diapycnal mixing (Gerdes, 1993; Roberts et al., 1996; Roberts and Wood, 1997). One approach has been to adopt the sigma-terrain following vertical coordinate (Phillips, 1957; Blumberg and Mellor, 1983; Gerdes, 1993). Howerver, this vertical coordinate introduces other known problems, such as pressure gradient errors and artificial diapycnal mixing. Winton et al. (1998) demonstrated that the problem of accurately representing downslope flows was

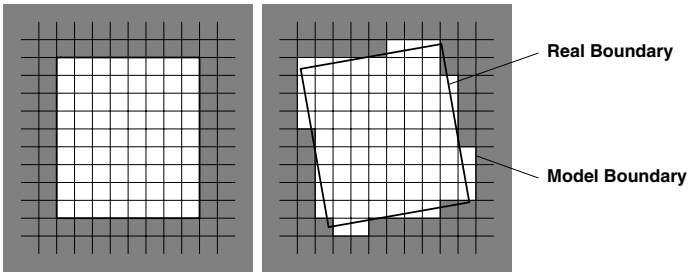

Fig. 1. Rotation of a square domain.

essentially a resolution problem. When the resolution in the vertical and the horizontal directions was high enough to represent the slope and the bottom boundary layer, an accurate simulation of the downsloping process was possible. Unfortunately, the resolution required is too high for conventional applications. On the other hand, specific parameterizations can remedy for the lack of resolution. For example, coarse resolution z-coordinate models may include an explicit bottom boundary model (Beckmann and Döscher, 1997; Lohmann, 1998; Killworth and Edwards, 1999). Additionally, Hirst and McDougall (1996) suggested that the turbulence scheme of Gent and McWilliams (1990) remarkably enhances the conservation of water properties as the water is advected down the slope. Although the physical processes involved may be different, there may be similar problems relating to the discretization of horizontal coastlines. That is, the presence of steps adjacent to energetic boundary currents may seriously compromise the dynamics of the model. The problem is exacerbated under free-slip, for which boundary currents tend to be stronger immediately adjacent to the coast. A question also arises regarding the influence of resolution versus the influence of steps. The smaller the grid cell, the larger the number of steps along a coastline. It is then not clear whether the solution becomes more accurate (due to higher precision in the interior) or less accurate (due to an increased number of singularities or steps along the boundary).

To date, there have been few studies focusing on this issue. Pedersen (1986) studied the influence of steps on gravity waves and found a retardation effect at coarse resolution. Schwab and Beletsky (1998) observed the same problem for Kelvin waves in different ocean models. AM addressed the problem in the context of the single gyre nonlinear Munk problem using a C-grid shallow water (SW) model. They showed (as did Cox, 1979) that the horizontal circulation under the no-slip boundary condition is not very sensitive to the presence of steps along the coastline. This can be explained by the fact that the core of the boundary current under no-slip is located a few grid points inside the interior of the basin.

For free-slip, however, they compared results from non-rotated and rotated square basin experiments and showed the circulation to be highly sensitive to the presence of steps along the walls. In rotated basin experiments, the basin was rotated relative to the grid axes (Fig. 1), but the wind forcing and north–south axis were kept constant relative to the basin, so that the only differences between the experiments are due to the discretization. The presence of steps along the boundary tends to reduce the strength of the circulation to the extent that results obtained using free-slip boundary conditions with step-like boundaries more closely resembles those with no-slip boundary conditions than free-slip solutions without steps. Moreover, they showed that, at least for small rotation angles, sensitivity to steps under free-slip conditions could be greatly reduced by using a vorticity–divergence formulation of the viscous stress tensor (Madec et al., 1991), hereafter referred as the δ–ζ formulation.

Our main objective is to refine results from AM by testing different numerical formulations of both the advective and diffusive terms, as we hypothesize that these terms are important from a vorticity budget point of view. Related changes to the overall circulation will be pointed as well. By using vorticity budgets, we also expect to quantify some of the results in AM. Finally, we point out that a similar problem of defining a vorticity budget exists in QG models (though with less dramatic consequences). This is may be a counter-intuitive result, since most of the QG models solve for the vorticity equation at second-order accuracy (that is, one order higher than a vorticity equation derived from the discretized at second-order primitive

equations would be). Results from QG models also help to shade some light on the shallow water experiments.

We conclude this introduction with three remarks. The first concerns the representation of the coastline in FD models. Some methods exist to treat exactly a coast not oriented along the discretization axes (Pember et al., (1995); Matthews et al., 1996; Forrer and Jeltsch, 1998). These methods have their own limitations, such as the treatment of viscous stresses at the boundary or time-step limitation problems. However, the emphasis of our study is not on developing or investigating these new FD models. Our focus is on testing the sensibility of step-like representations used in the ocean modelling community.

The second issue relates to the kind of idealized experiments we have performed. We have deliberately introduced artificial steps in the model boundary in these experiments. It is hoped that our results will give insight to the more relevant case where artificial steps result from real irregularities in coastine geometries. We should also comment that we expect the coastline problem described in this manuscript to have analogies with problems relating to steps appearing in the discretization of the shelf break in three-dimensional models.

Lastly, we decide to focus on the free-slip boundary condition because of the dramatic sensivity of the model solution to the presence of steps (as shown by AM) under this boundary condition. Even though the no-slip condition is more popular, it remains unclear why this choice should be the most appropriate, particularly at coarse resolution, but arguably also at the state-of-the-art resolution used in basin scale general circulation models.

The article is organized as follows. In Section 2, we compare the analytic vorticity budget with the equivalent discretized model vorticity budget for the SW model. We also show model vorticity budgets for various simulations and discuss the implications. Section 3 repeats the same approach for the QG model. Finally, a discussion and conclusions are given in Section 4.

2. Vorticity budgets in a C-grid SW model

In this section, we compare the analytic vorticity budget with the equivalent discretized vorticity budget for a C-grid shallow water (SW) model and explain why the two budgets do not match. We then give results for the discretized vorticity budget and discuss the implications in terms of modelling of wind-driven gyres in the presence of step-like coastlines.

The parameters we chose to use (see Appendix) lead to the following length scales (following scalings of Pedlosky, 1996, and others): The thickness of the Munk boundary layer (L_M) is 35 km and the thickness of the inertial boundary layer (L_I) is 43 km. This leads to a boundary layer Reynolds number (R_e) of 1.85 and a viscous sublayer of width 25 km. Due to the use of a reduced gravity coefficient, the Rossby radius of deformation is 31 km which is on the order of the resolution of our coarser grids. Therefore the steps may affect the mesoscale transients in our experiments. However, our solutions converge towards stationary equilibria, as is typical for the one-layer (with or without reduced gravity) single problem problem under free-slip conditions. That is, mesoscale transients tend to be negligible in our runs.

2.1. *The general form of the discretized vorticity budget*

We consider the shallow-water equations

$$\partial_t \mathbf{u} + \mathbf{u}\cdot\boldsymbol{\nabla}\mathbf{u} + f\mathbf{k}\times\mathbf{u} + g'\boldsymbol{\nabla}h = \frac{\boldsymbol{\tau}}{h} + \nu\nabla^2\mathbf{u} \quad (1)$$

$$\partial_t h + \boldsymbol{\nabla}\cdot(\mathbf{u}h) = 0 \quad (2)$$

where the variables are given in Table 1 and parameters in Appendix. It is sometimes convenient to recast the non-linear terms in eq. (1) in the following form:

$$\partial_t \mathbf{u} + q\mathbf{k}\times(\mathbf{u}h) + \boldsymbol{\nabla}B = \frac{\boldsymbol{\tau}}{h} + \nu\nabla^2\mathbf{u}, \quad (3)$$

where q and B are also given in Table 1. The kinematic boundary condition is no normal flow and the dynamic boundary condition is taken to be free-slip. The vorticity equation is found by taking the curl of eq. (3),

$$\partial_t\zeta + \boldsymbol{\nabla}\cdot(qh\mathbf{u}) = \mathbf{k}\cdot\boldsymbol{\nabla}\times\left(\nu\nabla^2\mathbf{u} + \frac{\boldsymbol{\tau}}{h}\right). \quad (4)$$

Upon integration of this equation over a closed basin, the divergence of the potential vorticity mass flux cancels out and we get

$$\partial_t\left(\int_\Omega \zeta\,\mathrm{d}x\,\mathrm{d}y\right) = \nu\oint_{\delta\Omega}\frac{\partial\zeta}{\partial n}\mathrm{d}l + \oint_{\delta\Omega}\frac{\boldsymbol{\tau}\cdot\mathbf{dl}}{h}. \quad (5)$$

Equations (1) and (2) or (2) and (3) can be discretized in different ways. To simplify the discussion,

Table 1. *List of variables in eqs. (1)–(3)*

$\mathbf{u} = (u, v)$	Horizontal velocity vertically averaged
$q = (\zeta + f)/h$	Potential vorticity
$\zeta = \mathbf{k} \cdot (\nabla \times \mathbf{u})$	Relative vorticity
$\mathbf{k} = (0, 0, 1)$	Unit vector normal to the horizontal plane pointing upward
h	Layer thickness (mean value = 1000 m)
f	Coriolis parameter
$B = g'h + \frac{1}{2}\mathbf{u} \cdot \mathbf{u}$	Bernoulli function
ν	Dynamic eddy viscosity
g'	Reduced gravity acceleration
$\boldsymbol{\tau}$	Wind stress in $m^2\ s^{-2}$ (i.e., normalized by density)
Ω	Basin domain
$\delta\Omega$	Boundary of the basin domain
$\mathbf{n}$	Normal vector oriented out of the domain
$\mathbf{C} = \mathbf{u} \cdot \nabla \mathbf{u} + f\mathbf{k} \times \mathbf{u}$	Advection–Coriolis terms

we leave the time derivative being continuous, and restrict ourselves to the C-grid. A useful general form of the SW equation is the following:

$$\partial_t u + C_u + \delta_x \Phi = \frac{\tau_u}{\overline{h}^x} + F_u \tag{6}$$

$$\partial_t v + C_v + \delta_y \Phi = \frac{\tau_v}{\overline{h}^y} + F_v \tag{7}$$

$$\partial_t h + \delta_x U + \delta_y V = 0 \tag{8}$$

where $\mathbf{C} = (C_u, C_v)$ represents the advection–Coriolis terms, Φ represents a potential function, $\mathbf{F} = (F_u, F_v)$ are the viscous terms and other notation is described in the Appendix. The exact forms of $\mathbf{C}$, Φ and $\mathbf{F}$ depend on choices made with respect to the discretization. For example, Φ might represent the Bernoulli function or simply the pressure, depending on whether a formulation based on eq. (1) or on eq. (3) is employed. We first make a general point about numerical vorticity budgets and later discuss the peculiarities specific to choices for $\mathbf{C}$, Φ and $\mathbf{F}$. From eqs. (6) and (7) we write the discretized vorticity equation

$$\partial_t \zeta = -\delta_x C_v + \delta_y C_u + \delta_x F_v - \delta_y F_u + \delta_x \left(\frac{\tau_v}{\overline{h}^y}\right) - \delta_y \left(\frac{\tau_u}{\overline{h}^x}\right). \tag{9}$$

This equation is defined at interior ζ-nodes only (i.e., excluding the boundary nodes), because it requires defining momentum equations at all neighboring velocity nodes (white squares in Fig. 2). We now want to sum over all interior ζ-indices in order to get the model vorticity budget. For simplicity, we write vectors in place of horizontal components, even though the components are not discretized at the same location (see Appendix):

$$\partial_t \sum_{ij \in \Omega_\zeta} \zeta \Delta x \Delta y = \sum_{ij \in \delta\Omega_\zeta} \left(-\mathbf{C} + \mathbf{F} + \frac{\boldsymbol{\tau}}{\overline{h}}\right) \cdot \boldsymbol{\Delta l}, \tag{10}$$

where $\delta\Omega_\zeta$ is the ensemble of indices representing the velocity nodes of the envelope of the interior vorticity node domain, Ω_ζ (black nodes in Fig. 2). We rewrite eq. (10) in a more convenient form by defining

$$\mathcal{F}_{\text{adv}} = -\sum_{ij \in \delta\Omega_\zeta} \mathbf{C} \cdot \boldsymbol{\Delta l}, \tag{11}$$

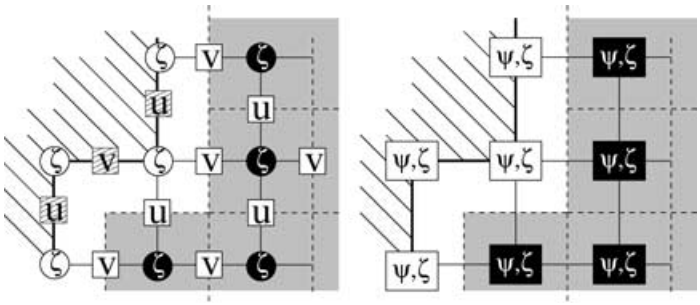

Fig. 2. Locations of variables near a step for the SW C-grid model (left panel) and for the quasi-geostrophic (QG) model (right panel). For the SW model, dashed squares are the boundary normal velocity nodes, white disks are the vorticity nodes where the relative vorticity is specified to be zero and black disks are the vorticity nodes for which a discretized vorticity equation can be written. In grey is the region delimiting the vorticity budget domain. This region does not extend to the model boundary. Instead, there is an half-cell band around the boundary (left in white) where we cannot derive any budget. A similar problem exists for the QG approximation.

$$\mathcal{F}_{\text{vis}} = \sum_{ij \in \delta\Omega_\zeta} \mathbf{F} \cdot \boldsymbol{\Delta}\mathbf{l}, \tag{12}$$

$$\mathcal{F}_{\text{i}} = \sum_{ij \in \delta\Omega_\zeta} \left(\frac{\boldsymbol{\tau}}{\overline{\overline{h}}} \right) \cdot \boldsymbol{\Delta}\mathbf{l}. \tag{13}$$

Thus eq. (10) becomes

$$\partial_t \sum_{ij \in \Omega_\zeta} \zeta \, \Delta x \, \Delta y = \mathcal{F}_{\text{i}} + \mathcal{F}_{\text{o}} = \mathcal{F}_{\text{i}} + \mathcal{F}_{\text{adv}} + \mathcal{F}_{\text{vis}}. \tag{14}$$

$\mathcal{F}_{\text{i}}$ (flux in) is the wind input of vorticity and $\mathcal{F}_{\text{o}}$ (flux out) is the sum of the viscous diffusion flux, $\mathcal{F}_{\text{vis}}$, and of the advective flux, $\mathcal{F}_{\text{adv}}$. The important point here is to note that $\mathcal{F}_{\text{adv}}$ ideally should be zero, since it represents an advective flux through the basin lateral boundary. It is not zero in the numerical model because the domain boundary for the model vorticity budget is located half a grid point inside the domain (Fig. 2). However, as the resolution increases, the region delimiting the vorticity budget domain approaches the model boundary, and $\mathcal{F}_{\text{adv}}$ should converge to zero. How quickly this occurs will depend on the numerical formulation.

It is always possible to approximate the vorticity budget at the model boundary by using off-centered derivatives and extrapolating or interpolating some of the variables to the boundary. However, we want to make sure that our vorticity budgets are relevant to the specific numerical formulation under investigation, especially since we hypothesize that the numerical formulation of the advective and diffusive terms (and the associated treatment of the steps) has an influence of the vorticity budget. Therefore, in order to investigate such an effect, we have to derive a budget from the discretized equations and to allow for a non-zero $\mathcal{F}_{\text{adv}}$ through the model vorticity budget boundaries.

One could argue that, physically, it is the vorticity budget integrated over the entire domain that is of interest, and that the advective contribution for this domain must vanish by virtue of the no normal flow condition. Also, because of the use of the free-slip boundary condition, the time tendency of the vorticity integral is not modified if the domain is chosen to be the model vorticity domain or the full model domain (for a straight wall free slip implies $\zeta = 0$ on the boundary; see next section for more details on vorticity boundary conditions). Moveover, for the form of the wind forcing chosen, its contribution to the vorticity budget is not significantly modified. Thus, the "full domain" vorticity budget should amount to a balance between $\mathcal{F}_{\text{i}}$ and a viscous flux of vorticity across the basin perimeter. It is not clear to us how to calculate this viscous flux in a way that is numerically relevant; however, we can always make an estimate using off-centered differencing. We tried a few reasonable schemes for estimating the viscous flux, and chose as "best" that for which $|\mathcal{F}_{\text{i}} + \mathcal{F}_{\text{vis}}|$ was smallest, i.e., for which the analytic vorticity budget was best satisfied. However, due to the use of second-order (only) numerics, it proved difficult to find an estimate of $\mathcal{F}_{\text{vis}}$ over the full domain which differs significantly from the value obtained over the model vorticity domain. As a consequence of this, there is an error in in our best estimate that is comparable in magnitude and sign to $\mathcal{F}_{\text{adv}}$. Presumably, the interpretation is that $\mathcal{F}_{\text{adv}}$ into the boundary strip leads to local convergence/divergence of vort in the strip, i.e., since $\mathcal{F}_{\text{adv}}$ must be zero on the wall. On physical grounds, this must be fluxed across the basin perimeter (in a steady state) by viscosity; however, we were not able to calculate this viscous flux independently. In other words, a large portion of $\mathcal{F}_{\text{vis}}$ remains unexplained (by our attempts to use off-center differencings to calculate it directly). Because we do not have a numerically relevant estimate of $\mathcal{F}_{\text{vis}}$ over the full domain, we prefer to concentrate on the cleaner, model vorticity domain budget which allows for a non-zero advection of vorticity, $\mathcal{F}_{\text{adv}}$.

Figure 3 compares the rotated and non-rotated basin cases. The corresponding circulation of the rotated basin case is plotted in Fig. 5A-20 km. The integrand of eq. (11) (i.e., the local $\mathcal{F}_{\text{adv}}$) is plotted as a function of distance around the basin perimeter and the position of the steps is evident from the abrupt jumps in the integrand value. When summed along the perimeter, $\mathcal{F}_{\text{adv}}$ is non-zero and is larger for the rotated basin experiment compared to the non-rotated basin experiment. Starting from this observation, we are interested in quantifying the importance of the steps over the global vorticity budget. First, as increased resolution leads to more steps, and due to the singular behavior of $\mathbf{C} \cdot \boldsymbol{\Delta}\mathbf{l}$ close to steps, it is no longer obvious that $\mathcal{F}_{\text{adv}}$ converges to zero with increasing resolution. Because of this, it seems reasonable to ask whether $\mathcal{F}_{\text{adv}}$ might be sensitive (perhaps even very sensitive) to the formulation of the advective terms in eq. (10), and by extension in equations (1) and (3). Second, we want to investigate whether the overall circulation is sensitive to the presence of an extra term in the global vorticity budget, as $\mathcal{F}_{\text{adv}}$ can be a source or a sink term, depending on its sign.

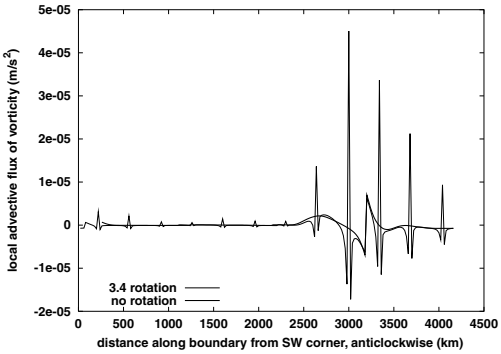

Fig. 3. Local advective flux along the boundary ($\mathbf{C}\cdot\boldsymbol{\Delta}\mathbf{l}/||\boldsymbol{\Delta}\mathbf{l}||$) at 20 km resolution in a square basin for the enstrophy conserving formulation of the advection using the B combination of Table 2. The heavy-lined curve is for no rotation of the basin, the light-lined curve is for a small angle rotation of the basin (3.4°) with respect to the grid. Due to the rotation angle, four steps occur along each side of the square and cause abrupt changes in the local advective flux. The circulation corresponding to the rotated case is plotted in Fig. 5A-20 km.

2.2. *Numerical formulations*

We are interested in applying different formulations for the advection–Coriolis terms since we noted that $\mathcal{F}_{\text{adv}}$ was generally non-zero for the single gyre Munk problem, with the integrand of eq. (11) being particularly large at steps. The two advective numerical schemes that we consider are the conventional formulation [based on eq. (1)] and the potential enstrophy conserving formulation [based on eq. (3)].

In addition to testing for sensitivity to the choice of advective schemes, we also consider different formulations of the stress tensor. That the overall circulation is particularly sensitive to the formulation of the stress tensor is the main result of AM, who found that the δ–ζ formulation gave better results than the conventional formulation. We refer to Gent (1993) and Shchepetkin and O'Brien (1996) for a more complete discussion on appropriate viscous stress tensor formulations for the shallow water equations, and limit ourselves to the two stress tensor formulations used by AM. Below, we review these two formulations. Thus, we are interested in testing four combinations of two advective and two diffusive formulations. Table 2 summarizes these four different combinations.

With respect to the advection–Coriolis terms, we compare the conventional formulation to the potential enstrophy conserving formulation of Sadourny (1975). For the conventional formulation, $\mathbf{C}$ and Φ are given by

$$\begin{cases} C_u = u\Delta_x u + \overline{\overline{v}^x}^y \Delta_y u - f\overline{\overline{v}^x}^y \\ C_v = \overline{\overline{u}^y}^x \Delta_x v + v\Delta_y v + f\overline{\overline{u}^x}^y \\ \Phi = g'h, \end{cases} \tag{15}$$

and for the potential enstrophy conserving formulation, $\mathbf{C}$ and Φ are given by

$$\begin{cases} C_u = -\overline{q}^y \overline{\overline{V}^x}^y \\ C_v = \overline{q}^x \overline{\overline{U}^x}^y \\ \Phi = g'h + \dfrac{1}{2}\left(\overline{u^2}^x + \overline{v^2}^y\right). \end{cases} \tag{16}$$

Both formulations ensure a second-order accuracy to the discretized SW equations. For the conventional formulation, changes are made to incorporate the boundary conditions[1] at second order of accuracy, by using off-centered differencings close to the boundary. The enstrophy conserving scheme explicitly uses the vorticity at boundary points. We choose to set the relative vorticity to zero along the model boundary, which is consistent with the free-slip boundary condition along straight walls[2]. Also, contrary to the conventional formulation, no off-centered differencing is needed at the boundary for the computation of $\mathbf{C}$.

The two numerical formulations that we consider for the viscous terms are the divergence–vorticity tensor formulation of Madec et al. (1991) and the

[1]The free-slip boundary condition is defined here as being the normal derivative of the tangential velocity set to zero. Other definitions are possible. For instance, Pedlosky (1987 p. 183) defines it as corresponding to being no viscous flux of tangential momentum across the boundary (i.e., $\nu[\partial v/\partial x + \partial u/\partial y] = 0$ at the wall). One might also consider zero vorticity at the coast as yet another definition of free slip. For the case of a straight coastline (with neither curvature nor artificial steps), these three definitions are equivalent.

[2]This choice was a matter of simplicity especially since the steps are artificial in this problem. It is pointed out that, depending on which of the three definitions of free slip is employed (see Footnote 1), the vorticity along the wall can be non-zero if curvature in the coastline is taken into account. In situations where steps arise as the result of complex basin forms, it may thus be necessary to rethink exactly how vorticity is specified at boundary nodes. A second point is that it is possible to specify non-zero vorticity at the tip of each step if the vorticity is computed in the usual fashion. This choice, however, tends to weaken the overall circulation, i.e., to make it less similar to the non-rotated basin solutions.

Table 2. *The four combinations of advection formulations and stress tensor formulations*

A	B	C	D
Enstrophy-preserving advection Conventional stress tensor formulation	Enstrophy-preserving advection δ–ζ stress tensor formulation	Conventional advection Conventional stress tensor formulation	Conventional advection δ–ζ stress tensor formulation

conventional five-point Laplacian. For the latter,

$$\begin{cases} \nabla^2 u_{ij} = \dfrac{u_{i-1,j} - 2u_{ij} + u_{i+1,j}}{\Delta x^2} \\ \qquad\qquad + \dfrac{u_{i,j-1} - 2u_{ij} + u_{i,j+1}}{\Delta y^2} \\ \nabla^2 v_{ij} = \dfrac{v_{i-1,j} - 2v_{ij} + v_{i+1,j}}{\Delta x^2} \\ \qquad\qquad + \dfrac{v_{i,j-1} - 2v_{ij} + v_{i,j+1}}{\Delta y^2}. \end{cases} \tag{17}$$

As with the conventional advection formulation, changes are made in eq. (17) to incorporate the boundary conditions at second-order accuracy, by using off-centered differencings.

Another technical remark concerns the treatment of velocity points close to tips of land, for these affect the computation of the Laplacian and the conventional advection terms. For those points (the u and v points of Fig. 4), the tip of the land is half a grid cell away. Let us focus on the u-point. The problem is to evaluate $\partial u/\partial y$ in the center of the northern side of the cell surrounding the u-point. The usual treatment would have

$$\left.\frac{\partial u}{\partial y}\right|_{\text{north}} = \frac{u_{i,j+1} - u_{ij}}{\Delta y} \tag{18}$$

which simplifies to

$$\left.\frac{\partial u}{\partial y}\right|_{\text{north}} = -\frac{u_{ij}}{\Delta y}, \tag{19}$$

because of the impermeability condition which sets $u_{i,j+1}$ to zero. Alternatively, one might take impermeability to imply that the tip is a stagnation point, in which case an off-centered differencing leads to

$$\left.\frac{\partial u}{\partial y}\right|_{\text{north}} = -\frac{2u_{ij}}{\Delta y}. \tag{20}$$

A third logical possibility would be to apply the free slip condition at the tip to conclude that

$$\left.\frac{\partial u}{\partial y}\right|_{\text{north}} = 0. \tag{21}$$

All three boundary condition may prove to be only first-order accurate close to the steps due to the discontinuous nature of the steps. As the grid spacing goes below L_I and L_M and the model geometry converges to the true geometry, we found that the choice of the exact treatment of the free-slip boundary condition does not substantially affect results. We nonetheless choose the third condition (21), in order to let the "fluid" slip as much as possible along the walls, since a desirable goal is to reduce the sensitivity of the circulation to the presence of artificial steps. [The first two conditions eqs. (19) and (20), tend to slow down the boundary currents at coarse resolution.] A more accurate (one that may prove to be second order) formulation of the boundary condition close to the steps can be derived using a finite volume formulation. This treats the northern viscous flux as a mean between eqs. (19) and (21). However, this formulation slows down the boundary current at coarse resolution

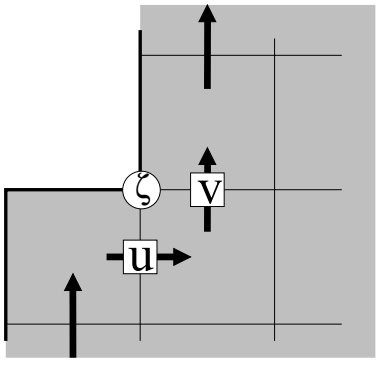

Fig. 4. Northward flow past a forward step. The shaded area is the model domain. We consider only the two momentum nodes for which the δ–ζ formulation differs from the conventional formulation. The ζ-point at the tip of the continent has $(i, j+1)$ indices. Arrows indicate direction of the flow.

due to the use of eq. (19). In addition, more accurate treatment of the steps have limited value, as the steps are artificial in this problem.

The divergence–vorticity (δ–ζ) form of the stress tensor leads to the following form for the Laplacians

$$\begin{cases} \nabla^2 u_{ij} = \delta_x D - \delta_y \zeta \\ \nabla^2 v_{ij} = \delta_y D + \delta_x \zeta \end{cases} \tag{22}$$

where $D = \delta_x u + \delta_y v$ is the divergence expressed at the h-location (center of the cell). This formulation is more general in the sense that there is no adjustment of the formulation at the boundary. Another remark concerns the case of straight walls. There, there is no difference between the δ–ζ stress tensor formulation and the traditional formulation. The difference is in the treatment of steps.

To illustrate this, we consider a comparison between the two stress tensor formulations for a forward step along a north-flowing western boundary current. Choose (i, j) so that, in Fig. 4, the ζ-point right at the tip of the land corner would have $(i, j + 1)$ indices (Fig. 15 for arrangement of indices). Thus, the viscous terms under the δ–ζ formulation are

$$\begin{cases} \nabla^2 u_{ij} = \text{conventional part} + \dfrac{v_{i,j+1}}{\Delta x \Delta y} \\ \nabla^2 v_{i,j+1} = \text{conventional part} + \dfrac{u_{ij}}{\Delta x \Delta y}, \end{cases} \tag{23}$$

where the additional terms are positive. These additional terms represent a forward acceleration. As AM noted, a serious inconvenience of the conventional formulation is that, in the presence of steps, there is "extra diffusion" of momentum due to additional velocity points set to zero at the boundary (the impermeability condition), as compared to the straight wall case. This extra diffusion is responsible for slowing down the boundary currents. Therefore, the accelerating terms of the δ–ζ formulation partly compensate the decelerating terms of the conventional formulation.

A final remark is that the divergence part of the viscous forces cancels out in the vorticity equation. Therefore, in the discretized vorticity equation, the δ–ζ formulation leads to a viscous term that takes the form of the five-point Laplacian of the vorticity. This is not true of the conventional formulation.

2.3. Results

By studying $\mathcal{F}_{\text{adv}}$, we want to address several issues related to the accuracy of the different combinations of the advection and diffusion formulations and their influence on the strength of the overall circulation. First, a major requirement is that, whatever the geometry of the basin, $\mathcal{F}_{\text{adv}}$ should converge to zero as the resolution goes to infinity. This test allows us to rank the performances of the model for the different combinations of advective and diffusive schemes. Of particular interest will be the importance of the advective formulation. A second concern is to assess whether the size of the artificial source or sink of vorticity due to $\mathcal{F}_{\text{adv}}$ influences the overall strength of the gyres. A third concern relates to the general accuracy of model vorticity budgets.

To address these issues, we make use of the conceptual experiment proposed by AM, in which a single gyre Munk circulation is computed in rotated and non-rotated square basins. In both cases, all parameters and forcing are unchanged except for the discretized coastline. The four combinations (A, B, C, D) of numerical formulations we propose to test are detailed in Table 2. One remark concerns the non-rotated basin results. There, since the conventional and δ–ζ stress tensor formulations are identical, the results for the B combination are identical to the results for A. The same applies for the C and D cases.

We reproduce qualitatively (different physical parameters were used) the results of AM in Fig. 5. All runs are 6 yr long, by which time the vorticity budget has reached an approximate equilibrium. The budget computations were carried out using the instantaneous fields at the end of the run. Using later fields do not lead to any significant differences. This figure shows the elevation fields for the A and B cases, and for no rotation and a small rotation angle of 3.4°. Clearly, the A case shows circulation patterns collapsing as the number of steps along the walls increases whereas, for the B case, the circulation is quite similar to the original non-rotated circulation. The results for C are not shown but are very similar to the results for A. The results for D show a small increase in the strength of the gyre compared to A, but the original overall circulation of A and B with no rotation is not recovered (not shown).

Figure 6a shows the total kinetic energy[3] as a function of resolution for the various combinations and for

[3]The kinetic energy in the SW equations can be defined as $1/2\ \mathbf{u}^2\ h$ which has units of $m^3\ s^{-2}$. The total kinetic energy being the basin-integrated kinetic energy then has the units of $m^5\ s^{-2}$. This explains the somewhat unconventional choice of units for the energy here.

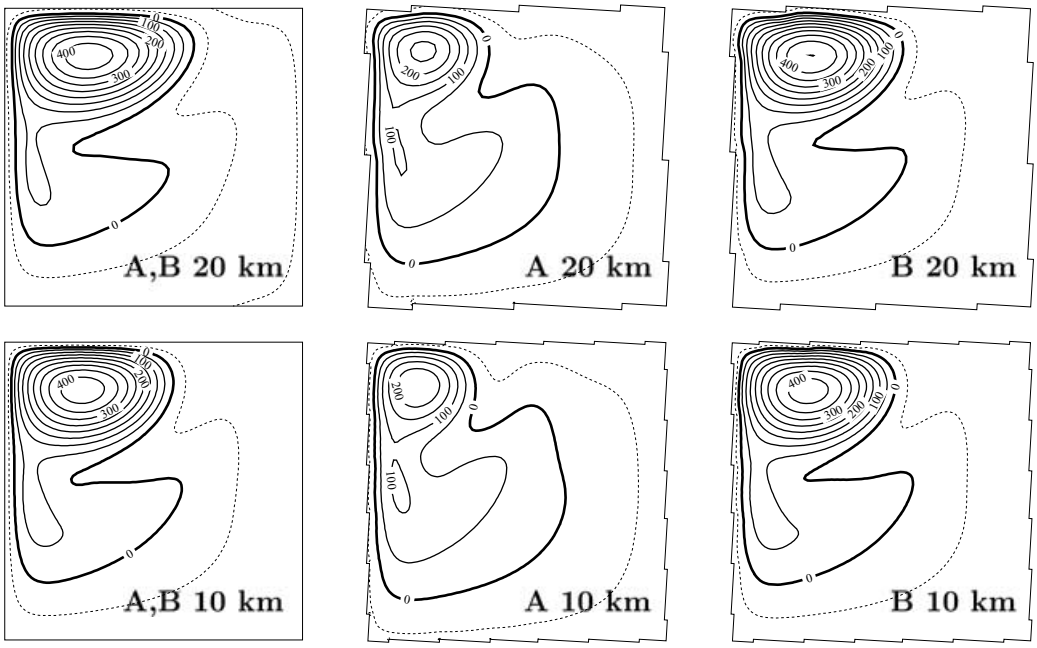

Fig. 5. Elevation fields in meters after a 6 yr spin-up for 20 and 10 km resolution. Shown are results from the A and B combination (Table 2) with or without a 3.44° rotation angle of the basin. Note that the B case tends to resemble the A,B case with no rotation, but not the A case.

a rotation angle of 3.4°. Only the B combination converges to non-rotated solutions. The A and C results are almost identical, but appear to converge to a kinetic energy that is reduced by over a factor of 2 compared to the non-rotated cases. For the D combination, kinetic energy decreases and then tends to increase slightly with increasing resolution and is generally much lower than for A and B with no rotation or B with rotation.

As mentioned, the first consistency test related to the vorticity budget is to verify that $\mathcal{F}_{\text{adv}}$ converges to zero with increasing resolution. For all rotation angles considered and for the B combination, this appears to be the case, i.e., $\mathcal{F}_{\text{adv}}$ does decrease to zero with increasing resolution. For the other combinations (A, C and D), such is not the case, at least for certain angles. For instance, $\mathcal{F}_{\text{adv}}$ tends to increase or stay constant

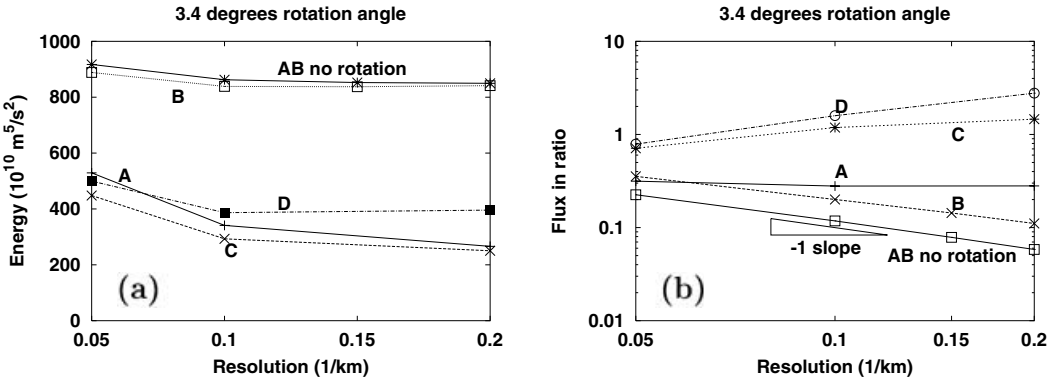

Fig. 6. (a) Kinetic energy after spin-up and (b) ratio of $\mathcal{F}_{\text{adv}}$ to $\mathcal{F}_{\text{i}}$ for the four combinations combinations. Results are shown for a 3.4° rotation angle of the basin. The A,B (no rotation) curve is also plotted for comparison.

for the A, C and D combinations at 3.4° (Fig. 6b). For the D case, $\mathcal{F}_{adv}$ increases dramatically with increasing resolution, so much that $\mathcal{F}_{adv}$ becomes larger than the wind input. Associated with this is a reverse (negative) viscous flux. This behavior may have consequences on the stability of the model. Although no obvious numerical instabilities occurred for a rotation angle of 3.4°, numerical instabilities cause the model to crash for other angles, for example at −30°. It seems plausible that this behaviour is associated with the large (and opposing) advective and diffusive fluxes of vorticity near the model perimeter. In any event, it seems reasonable to conclude that the D combination is inappropriate. This implies that the δ–ζ viscous formulation performs well only when used in conjunction with the enstrophy-conserving advection. This finding complements that of AM. For the A and C combinations (Fig. 6b), $\mathcal{F}_{adv}$ does not converge toward zero with increasing resolution. Hence, these two combinations seem inappropriate, even if the resulting solutions are always stable.

We now address the issue of possible correlation between $\mathcal{F}_{adv}$ and the kinetic energy. Given that inertial runaway[4] appears to be related to "difficulties" in balancing the global vorticity budget (Pedlosky, 1996), it seems reasonable to ask whether the sign of $\mathcal{F}_{adv}$ is correlated with an indicator of the overall strength of the gyre, such as total kinetic energy. For example, when $\mathcal{F}_{adv}$ is negative, it adds to the wind input of vorticity and one might expect a stronger gyre to result. Some evidence that this may be the case is found by comparing B and D, which share the same formulation of the viscous terms. Figure 6b shows that $\mathcal{F}_{adv}$ is positive and larger for D than is the case for combination B. Thus the total wind plus advective input of vorticity to the basin is stronger in case B. As might have been anticipated, B shows a more energetic circulation (Fig. 6a). It is also interesting to see whether there is any correlation between kinetic energy and the sign/strength of $\mathcal{F}_{adv}$ for a given formulation of the numerics. We restrict this discussion to the use of the B combination. From Figs. 7 and 8, which show the kinetic energy and advective/wind vorticity input ratio for a range of resolution and rotation angles, there does not appear to be any striking correlation. In particular, if we focus on the region of negative values of $\mathcal{F}_{adv}$ (i.e., for a case where $\mathcal{F}_{adv}$ has the same sign as the wind input), the kinetic energy for this region is not larger than the kinetic energy at the same resolution but for an opposite angle (in fact, the kinetic is slightly lower). Presumably the added advective flux in this region is locally balanced by the viscous terms, so that processes analogous to those thought to be responsible for inertial runaway do not lead to an increase in the overall strength of the gyre.

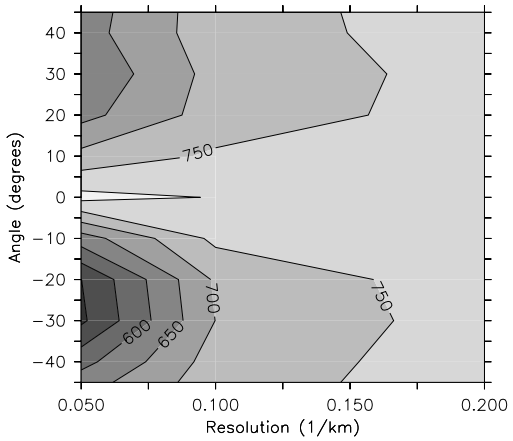

Fig. 7. Kinetic energy after spin-up for the B combination in 10^{10} m^5 s^{-2}.

To conclude this section, we investigate the general accuracy of model vorticity budgets with respect to $\mathcal{F}_{adv}$ using the B combination only, since this combination is the only one showing a robust convergence to zero with increasing resolution. As $\mathcal{F}_{adv}$ should

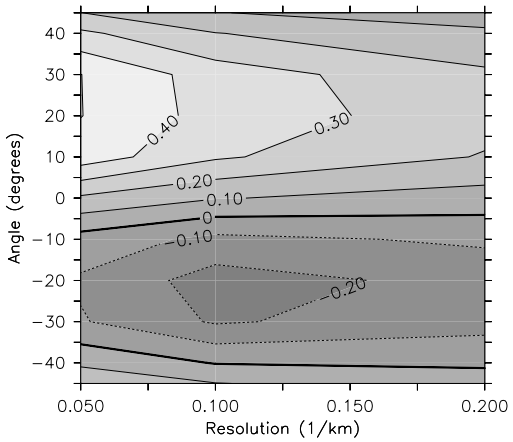

Fig. 8. Ratio of $\mathcal{F}_{adv}$ to $\mathcal{F}_i$ for the B combination.

[4]Defined as the inability of simple models of the ocean to converge to a reasonable statistical mean solution as frictional parameters as the eddy viscosity are reduced.

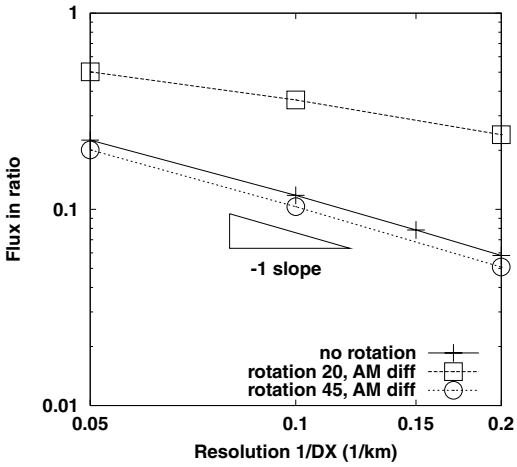

Fig. 9. Convergence of $\mathcal{F}_{\text{adv}}$ with resolution for 0, 20 and 45° rotation angle for the B combination.

ideally not be present in the vorticity budget, the viscous flux, $\mathcal{F}_{\text{vis}}$, can be either underestimated or overestimated (which modifies the local balance at the wall and therefore the strength of the gyre), and $\mathcal{F}_{\text{adv}}$ can be viewed as an error. From Fig. 9 and for the range of resolution we used, $\mathcal{F}_{\text{adv}}$ varies between 5% and 50% of the wind input. The order of the convergence for $\mathcal{F}_{\text{adv}}$ with increasing resolution is fairly close to unity or slightly lower for all positive angles. For negative angles, we did not compute the convergence order because $\mathcal{F}_{\text{adv}}$ goes through a minimum (Fig. 8) and had not asymptoted to an uniform convergence order at the highest resolutions we considered. A noteworthy point is that the effect of increasing the rotation angle (introducing more steps) seems to decrease the convergence order (to 1/2 for a 20° rotation angle). Paradoxically, however, the convergence order increases again to reach unity for 45°, the rotation angle at which the number of steps is maximum. In fact, at this angle $\mathcal{F}_{\text{adv}}$ even shows lower values compared to the 0° angle.

Except for effects related to step-like boundaries, that the convergence order is unity follows directly from the order of discretization of the vorticity. Since the vorticity is one order higher a variable than is velocity, and since the velocity is computed at second-order accuracy, it follows that the vorticity is at best accurate to first order. Therefore, $\mathcal{F}_{\text{adv}}$ can be considered an explicit first order (at best) error in the vorticity budget. For the B combination, we observe that the convergence order for $\mathcal{F}_{\text{adv}}$ varies between 1/2 and unity, depending on the rotation angle. In the 1/2-order case, errors (or discrepancies) vary between 25% (high resolution) and 50% (coarse resolution) and, in the first-order case, they vary between 6% and 22%. The errors are much larger for the other combinations and can reach 100%. This implies that the accuracy of computing vorticity budgets from primitive equations models is fairly low, especially in the absence of attention to the numerics. These errors may also vary considerably with the discretized domain geometry.

3. The quasi-geostrophic model

3.1. Discretization

We also investigated the influence of coastline discretization in quasi-geostrophic (QG) models. QG models solve the vorticity equation directly. It therefore seems a reasonable assumption that these models should yield more accurate vorticity budgets than do SW and primitive equation models. The vorticity equation used is

$$\partial_t \zeta + J(\psi, \zeta) + \beta \partial_x \psi = \nu \nabla^2 \zeta + \mathbf{k} \cdot \boldsymbol{\nabla} \times (\boldsymbol{\tau}/h), \tag{24}$$

where ψ is the streamfunction, and the layer thickness, h, is proportional to ψ[5]. Other notation is standard. In all experiments, the discretization of eq. (24) is done using second-order center differencings, and a simple leapfrog scheme was used to time step the vorticity. The viscous term is discretized by the conventional five-point Laplacian, and the free-slip boundary condition is applied by setting the vorticity boundary nodes to zero. We focus on testing different formulations of the Jacobian in eq. (24), as the formulation of this term may have consequences for the vorticity budget for the same reasons mentioned previously for the C-grid model. The free-slip boundary condition is applied by setting the vorticity boundary nodes to zero.

As with the SW C-grid model, the vorticity budget for the QG model is defined only on an interior

[5]We also did some experiments with more standard QG forcing (i.e., without the variable h on the r.h.s), and saw no significant changes. The variable h was kept here so as to better mimic our SW experiments. In the same spirit, we did some experiments with a reduced-gravity, free-surface version of this code. Once again, our major conclusions did not appear to be affected.

sub-domain, half a grid point inside the model basin. This follows from the fact that the vorticity equation is only solved at interior points (Fig. 2). In this subdomain, discretization of the vorticity budget is straightforward, except that the advective contribution, $\mathcal{F}_{\text{adv}}$, includes one part associated with the Jacobian, and another associated with the β term. This β contribution is hidden in $\mathcal{F}_{\text{adv}}$ for the SW models. Therefore, we define $\mathcal{F}_{\text{adv}}$ here to be $\mathcal{F}_{\text{adv}} = \mathcal{F}'_{\text{adv}} + \mathcal{F}_{\text{c}}$, where $\mathcal{F}'_{\text{adv}}$ represents the integration of the Jacobian term over the ensemble of interior nodes, Ω_ζ. Thus, by analogy with eq. (14), we recast the vorticity budget in the following form

$$\sum_{ij\in\Omega_\zeta} \partial_t \zeta \,\Delta x \,\Delta y = \mathcal{F}'_{\text{adv}} + \mathcal{F}_{\text{c}} + \mathcal{F}_{\text{vis}} + \mathcal{F}_{\text{i}}. \tag{25}$$

We focus our study on the behavior of both $\mathcal{F}'_{\text{adv}}$ and $\mathcal{F}_{\text{c}}$. As for the C-grid model, a minimum requirement is that $\mathcal{F}_{\text{adv}}$ goes to zero at infinite resolution. Here, this also applies to $\mathcal{F}'_{\text{adv}}$ and $\mathcal{F}_{\text{c}}$ separately. Representation of the Jacobian in eq. (25) has been extensively considered by Arakawa (1966) and Arakawa and Lamb (1977, hereafter, AL77). From the latter, we borrow the notation J_i, where J is the discretized Jacobian and i takes values between 1 to 7, depending on the discretized formulation. We propose to test three different numerical formulations of the Jacobian, J_1, J_3 and J_7, and investigate their respective influence on the vorticity budget. J_7 is also refered to as the Arakawa Jacobian.

The simplest representation is the J_1 Jacobian, where

$$J_1 = \Delta_x \zeta \,\Delta_y \psi - \Delta_y \zeta \,\Delta_x \psi. \tag{26}$$

The notation is found in the Appendix. J_1 conserves relative vorticity in doubly periodic domains, straight channels and rectangular domains when the free-slip boundary condition is applied. In fact, $\mathcal{F}'_{\text{adv}}$ is zero for zero rotation angle because ψ and ζ are both zero at the boundary. However, it has poor conservation properties for both energy and enstrophy. Additionally, we noted that when J_1 is used, solutions are very different for positive and negative values of the rotation angle of the basin. Positive angles are characterized by larger kinetic energy and stronger oscillations of a Rossby basin mode (not shown). This is particularly true at low to moderate resolutions, with model behaviour improving for higher resolutions. Because of its poor behaviour at moderate resolutions, and because its poor conservation properties, we prefer to discard this formulation of the Jacobian for the rest of the discussion.

AL77 proposed the J_3 form of the Jacobian which conserves energy in doubly periodic domains

$$J_3 = \Delta_x(\zeta \,\Delta_y \psi) - \Delta_y(\zeta \,\Delta_x \psi). \tag{27}$$

The J_3 Jacobian conserves relative vorticity in doubly periodic domains, but not in the presence of boundaries. The boundary terms that arise are relatively easy to pinpoint. They correspond to the value $\zeta \,\Delta_y \psi$ or $\zeta \,\Delta_x \psi$ at locations one grid point away from the boundaries.

The last Jacobian formulation we propose to test is the J_7. This more intricate formulation (Arakawa, 1966) is known to conserve both the energy and the enstrophy in doubly periodic domains. The J_7 Jacobian also conserves relative vorticity in doubly periodic domain, but not in closed domains where complicated boundary terms in $\mathcal{F}'_{\text{adv}}$ arise. This formulation is very popular and is adopted in most QG models.

Finally, we note that the viscous term in the SW vorticity equation derived using the δ–ζ stress tensor formulation is similar to the viscous term in the QG equation. Specifically, both take the form of a five-point Laplacian of vorticity. Additionally, the divergence form of J_3 makes it analogous to the divergence form of the potential vorticity advection formulation of Sadourny (1975) for use in the SW vorticity equation. Hence, we expect that the results of the J_3-QG model should be similar to those of the SW model using the B combination. (Unfortunately, there is no straightforward analog between the conventional advection formulation for the C-grid and any of the Jacobian operators suggested by AL77.)

3.2. *Results*

Solutions using J_3 and J_7 appear stable and converge reasonably well with increasing resolution to the same value of kinetic energy, for both rotated and non-rotated basins (Fig. 10). Thus, at least for the J_3 and J_7 formulations, the QG model appears to be less sensitive to grid rotations. With respect to the vorticity budget, we are interested in the behavior of the advective contribution, $\mathcal{F}_{\text{adv}}$, with increasing resolution. As mentioned, $\mathcal{F}_{\text{adv}}$ is made of two independent contributions, $\mathcal{F}'_{\text{adv}}$ and $\mathcal{F}_{\text{c}}$. $\mathcal{F}'_{\text{adv}}$ depends directly on the Jacobian formulation but $\mathcal{F}_{\text{c}}$ does not. Figure 11 shows the convergence of $\mathcal{F}'_{\text{adv}}$ in rotated and non-rotated basins for the two Jacobians considered. $\mathcal{F}'_{\text{adv}}$

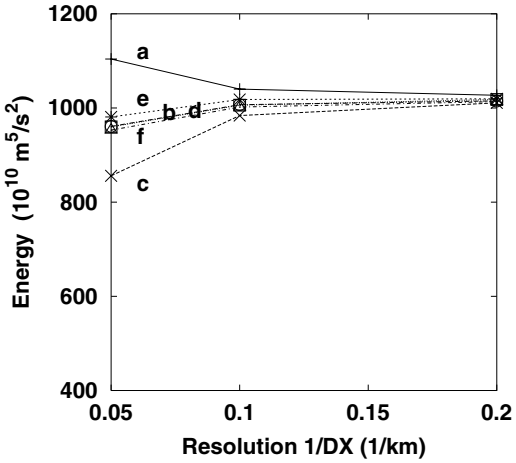

Fig. 10. Kinetic energy after spin-up for (a) J_3 at 0° rotation, (b) J_7 at 0°, (c) J_3 at 30°, (d) J_7 at 30°, (e) J_3 at −30°, (f) J_7 at −30°.

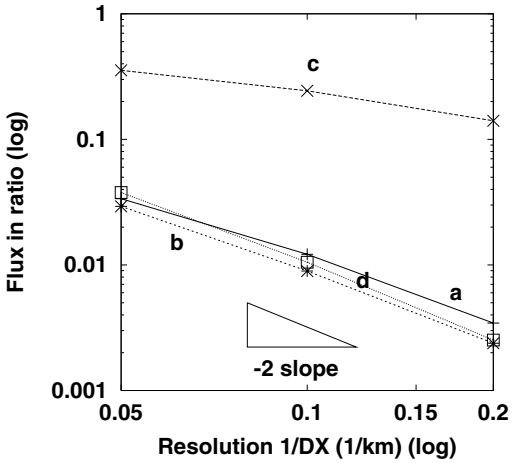

Fig. 11. Ratio of $\mathcal{F}'_{\text{adv}}$ to the wind input for (a) J_3 at 0° rotation, (b) J_7 at 0°, (c) J_3 at 30°, (d) J_7 at 30°.

is close to second order in non-rotated basins for both Jacobians. At 30° rotation, however, the convergence order is closer to unity for J_3 but second order for J_7.

Figure 12 shows the convergence for $\mathcal{F}_{\text{c}}$ in rotated and non-rotated basins under J_3 and J_7. The results appear independent of the Jacobian formulation, as expected. The convergence order is, however, unity, in contrast with results for $\mathcal{F}'_{\text{adv}}$ (Fig. 13). This result comes readily from the traditional treatment of the β term. The proof is given in a square domain:

$$\beta \sum_{ij\in\Omega_\zeta} \Delta_x\psi\,\Delta x\Delta y = \beta \sum_j \sum_{i=2}^{i=n_x-1} \frac{\psi_{i+1}-\psi_{i-1}}{2\Delta x}\Delta x\Delta y$$

$$= \beta \sum_j \frac{\psi_{n_x-1}-\psi_2}{2}\Delta y, \qquad (28)$$

since $\psi_1 = \psi_{n_x} = 0$, by definition of non-permeability. The west–east asymmetry due to the beta effect imposes that $\psi_{n_x-1} = a\psi_2$ with $0 < a < 1$

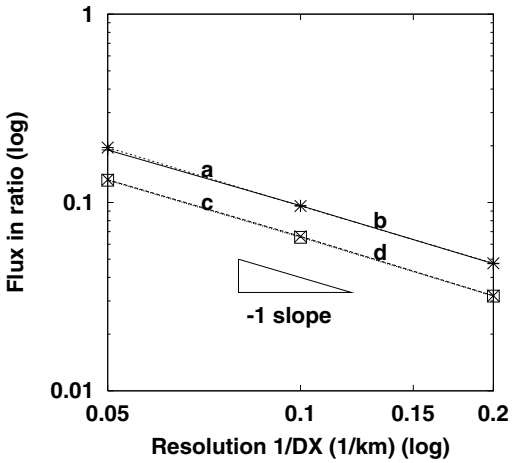

Fig. 12. Ratio of $\mathcal{F}_{\text{c}}$ to the wind input. (a–d) as described in Fig. 10.

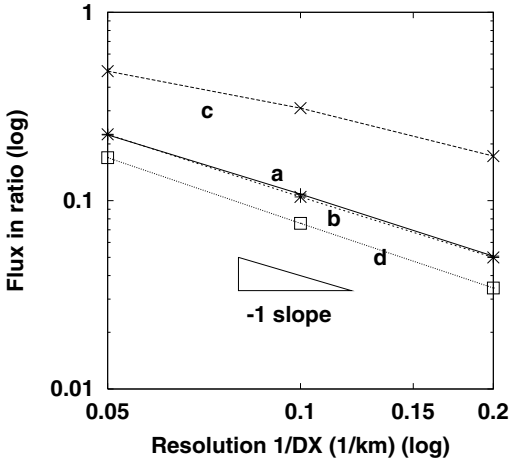

Fig. 13. Ratio of $\mathcal{F}_{\text{adv}} = \mathcal{F}'_{\text{adv}} + \mathcal{F}_{\text{c}}$ to the wind input. (a–d) as described in Fig. 10.

and all other parameters kept constant. The factor, a, represents the ratio of the velocity along the west and east coastline. Because ψ_{n_x-1} and ψ_2 converge linearly to zero with increasing resolution, the beta contribution cannot have a better convergence rate than one. In absolute value, $\mathcal{F}_c$ is also larger than $\mathcal{F}'_{adv}$. Therefore, $\mathcal{F}_{adv}$ suffers primarily from the low convergence rate of the beta contribution, $\mathcal{F}_c$. One can ask whether we can get a better convergence order by including the planetary vorticity, βy in the Jacobian instead of treating it separately [$J(\psi, \zeta + \beta y)$ instead of $J(\psi, \zeta) + \beta\partial_x\psi$]. We conducted this experiment with the best advective formulation, J_7. However, the convergence order of $\mathcal{F}_{adv}$ is again unity and errors are very similar to the previous case (not shown).

One last point we would like to make is related to similarities mentioned above, between the J_3-QG and the B combination of the SW model. Figure 14 shows $\mathcal{F}'_{adv}$, $\mathcal{F}_c$ and $\mathcal{F}_{adv}$ with increasing resolution for J_3 and under -30° rotation angle. $\mathcal{F}'_{adv}$ is negative, goes through an minimum and then increases toward zero, whereas $\mathcal{F}_c$ is positive and decreasing to zero. Hence, $\mathcal{F}_{adv}$ appears to go through a pool of negative values, just as the B results showed. This contrasts with results using J_7, for which $\mathcal{F}'_{adv}$ takes positive values for both negative and positive rotation angle (not shown).

To conclude, except for the J_1 Jacobian, the QG model is less sensitive to the basin rotation than is the SW model. Convergence orders for the advective flux of vorticity, $\mathcal{F}_{adv}$, on the other hand, are order 1 or less, comparable to what was found for the SW simulations. In the QG case, this low order of convergence is related to the beta contribution, $\mathcal{F}_c$. Using J_7, $|\mathcal{F}_{adv}|$ varies between 5% (high resolution) and 20% (coarse resolution) of the wind input, depending on the rotation angle. These results are somewhat better than those obtained in the SW simulations.

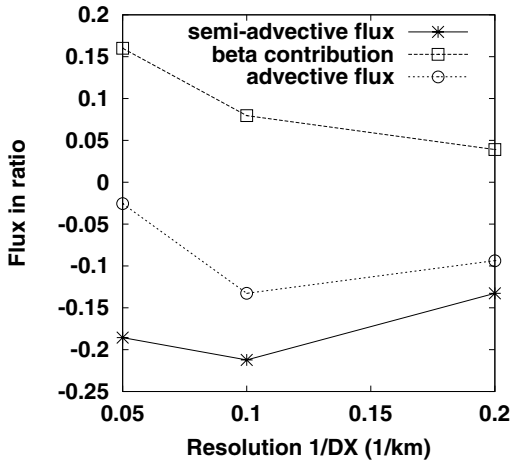

Fig. 14. Semi-advective flux, $\mathcal{F}'_{adv}$, and beta contribution, $\mathcal{F}_c$, to the vorticity budget for the J_3 Jacobian at -30° rotation angle. $\mathcal{F}_{adv} = \mathcal{F}'_{adv} + \mathcal{F}_c$ is negative at this rotation angle, similar to results obtained for the B combination.

4. Discussion and conclusion

Due to their fractal nature, realistic coastlines will inevitably have features down to the model resolution. While the ultimate goal would be to correctly account for such features in models, a less stringent test is that models should be able to deal with simple geometries, in a manner that is not sensitive to artificial steps introduced by the discretization. Such was the study of AM, based on free-slip and no-slip single gyre Munk experiments. Noting an inconsistency in the discretized vorticity budget for the C-grid shallow water model, we decided to revisit the AM results in terms of global vorticity budgets with varying resolution. Our goal was to investigate the influence of the formulation of the advective and viscous terms on the model vorticity budget and the overall strength of the gyre.

AM showed that the conventional viscous stress tensor formulation was inappropriate in the rotated basin case, for steps occurring along the coast. Moreover, they made use of an alternative stress tensor formulation (herein called the δ–ζ tensor) and showed improved results. We further analyzed the difference between conventional and δ–ζ tensor formulation along with two different formulations for the advection in the momentum equations in terms of global vorticity budgets with varying resolution. One observation is that the results with the δ–ζ stress tensor depend strongly on the formulation of the advection, as the conventional advection formulation leads to instability (the D combination). Therefore, the formulation of the advection seems equally important in explaining the AM results. In terms of vorticity budgets, all combinations seem to be ill-behaved except for the enstrophy conserving advection and the δ–ζ tensor (the B combination). For this combination, the convergence order for $\mathcal{F}_{adv}$ is about unity, following the truncation order of the vorticity when derived from second-order velocity. We also discussed various boundary treatments

of the normal gradient of the tangential velocity when using the conventional advection and viscous tensor. Formally at least, none of these are known a priori to be better than first order in the presence of steps, so that zeroth-order errors in the vorticity budget may explain the results for combinations A, C and D. A formally second-order finite volume formulation of the steps [an average of eqs. (19) and (21)] using both the conventional advection and viscous tensor was also tried and gave results very similar to combination A (i.e., no improvement.) Note, however, that this second-order treatment is for a geometry for which the steps are considered to be "real".

For the QG model, the overall circulation is less sensitive to the rotation of basin for two Jacobians of the three we tried. In order of increasing accuracy, J_1 gives the lowest level of accuracy (showing even signs of instability at low resolution), followed by J_3 and then J_7. The best convergence order for $\mathcal{F}'_{\text{adv}}$ was obtained by using the J_7 Jacobian and was about 2, for all rotation angles. The beta contribution, $\mathcal{F}_{\text{c}}$, is independent of the formulation of the Jacobian. Its convergence order is very close to unity, and its magnitude is usually larger than that of $\mathcal{F}'_{\text{adv}}$. Therefore, most of the discrepancy between the real and the model vorticity budgets is concentrated in the beta contribution at sufficiently high resolution. Hence, in order to make accurate vorticity budgets, it follows that the beta contribution should be more accurately computed. One possibility is to increase the order of the finite differencing operator for the beta term, $\beta\partial_x\psi$. Finally, the hypothesis that the J_3-QG model would give similar results compared to the enstrophy-conserving advection and the δ–ζ tensor C-grid model was verified.

From the general point of view of computing vorticity budgets from finite difference models, both the QG and C-grid models show the same relatively slow convergence order (about unity) of the discrepancy with increasing resolution between the real and the model vorticity budgets. For the range of resolution considered, and depending on the model type (SW or QG), numerical formulations and the rotation angle (or more generally, basin geometry), this "truncation" error can be estimated to vary between 5 and 50%.

We expect these results to be of relevance to basin scale vorticity budgets computed from general circulation model (GCM) output. Of particular concern are coarse models using large viscous eddy coefficients. There, the basin vorticity budget should be considered with caution. Most of these models use the no-slip boundary condition, although a convincing argument from first principles that this is the "correct" boundary condition appears lacking. For reasons outlined in the introduction, we have concentrated here on the free-slip condition. However, given the widespread use of no slip, we also carried out a few additional experiments using no slip. These show that the truncation error converges faster in all cases (between first and second order), and this seems to be related (in the QG context) to the streamfunction approaching zero parabollicly. [The latter result can be obtained using the same argument we used for free slip, i.e. eq. (28).] Finally, we might speculate as to how the choice of advective and dissipative numerical formulations may affect results in a more realistic setting. Recall that for the square basin geometry, "improper" representation (in the presence of artificial steps) can cause free-slip solutions to become less energetic, to the point where they start to resemble their no-slip counterparts. Given that artificial steps are unavoidable (for finite difference methods) when complex geometries are considered, it would then seem plausible, for example, that use of the B combination (in a C-grid primitive equation model) should produce circulations that are both more energetic (particularly near boundaries) and have better convergence properties than would be the case for the other combinations that we considered. We should caution, however, that when geometries having sharp coastlines are considered, curvature in the boundary may lead to enhanced viscous vorticity fluxes across the basin perimeter. Results from a spectral element model (Dupont, 2001, chap. 5) suggest that this leads to a slowing of the overall circulation, depending on the precise definition of free slip (see Footnote 1, Section 2.2). It is important that the slowing in this case, however, results from resolved features of the circulation and the coastline, rather than from poor representation of the numerics. Similar studies, in more complex basin geometries, are needed to assess the degree to which the issues considered here might affect GCM results for realistic basin geometries.

5. Appendix

Notation and parameters for the discretized equations on a C-grid and for the QG model

Here will be found the notations and values of parameters used for the discretized equations on C-grid and for the QG model. Figure 15 shows the physical

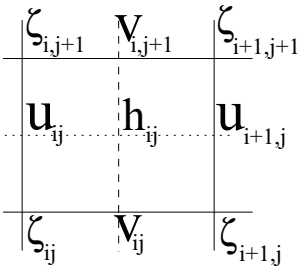

Fig. 15. Indices for u, v, h and ζ on the C-grid.

locations of the different indices for the u, v, h and ζ variables on the C-grid.

List of parameters and variables:

u and v are the horizontal velocity components (East and North) and h is the depth of the fluid;

δ_x, Δ_x, are approximated by the following central differencing operators (and similarly for the y-operators)

$$\delta_x\phi(x, y) = \frac{\phi\left(x + \frac{\Delta x}{2}, y\right) - \phi\left(x - \frac{\Delta x}{2}, y\right)}{\Delta x}, \tag{29}$$

$$\Delta_x\phi(x, y) = \frac{(\phi x + \Delta x, y) - (\phi x - \Delta x, y)}{2\Delta x}; \tag{30}$$

$\overline{\phi}^x$ is a double point average $= \frac{1}{2}(\phi_{ij} + \phi_{i-1,j})$. A similar definition applies to $\overline{\phi}^y$;

$q = (f + \zeta)/\overline{\overline{h}^x}^y$ with $\zeta = \partial_{x-}v - \partial_{y-}u$;

$U = u\overline{h}^x$, $V = v\overline{h}^y$;

$B = g'h + \frac{1}{2}(\overline{u^2}^x + \overline{v^2}^y)$;

F_x and F_y are the viscous forces.

f is defined at 45° North at the center of the domain;

$g\prime = 0.01$ m s^{-2}, $L_{\text{Rossby}} = 31.22$ km;

$L_x = L_y = 1000$ km are the lengths of the basin;

$\tau_u = -10^{-4}\cos(\pi \times y/L_y)$, $\tau_v = 0$, single gyre forcing. Units are in m^2 s^{-2}.

REFERENCES

Adcroft, A. and Marshall, D. 1998. How slippery are piecewise constant coastlines in numerical ocean models. *Tellus* **50-A**, 95–108.

Arakawa, A. 1966. Computational design for long-term numerical integration of the equations of fluid motion: Two-dimensional incompressible flow. part 1. *J. Comput. Phys*. **1**, 119–143.

Arakawa, A. and Lamb, V. R. 1977. Computational design of the basic dynamical processes of the UCLA general circulation model. *Meth. Comput. Phys*. **17**, 174–267.

Beckmann, A. C. and Döscher, R. 1997. A method for improved representation of dense water spreading over topography in geopotential-coordinate models. *J. Phys. Oceanogr*. **27**, 581–591.

Bleck, R. and Boudra, D. B. 1981. Initial testing of a numerical ocean circulation model using a hybrid quasi-isopycnal vertical coordinate. *J. Phys. Oceanogr*. **11**, 755–770.

Blumberg, A. and Mellor, G. 1983. Diagnostic and prognostic numerical circulation studies of the south atlantic bight. *J. Geophys. Res*. **88**, 4579–4592.

Bryan, K. 1969. A numerical method for the study of the circulation of the world ocean. *J. Comput. Phys*. **4**, 347–376.

Cox, M. D. 1979. A numerical study of somali currents eddies. *J. Phys. Oceanogr*. **29**, 311–326.

Cox, M. D. 1984. A primitive equation three-dimensional model of the ocean. Tech. Rep., GFDL Ocean Group, NOAA, Princeton Univ., Princeton, NJ.

Dietrich, D. E. Ko, D.-S. and Yeske, L. 1993. On the application and evaluation of the relocatable DieCAST ocean circulation model in coastal and semi-enclosed seas. Tech. Rep. 93-1, Center for Air Sea Technology, Mississippi State University, Building 1103, Stennis Space Center, MS 39529.

Dupont, F. 2001. *Comparison of numerical methods for modelling ocean circulation in basins with irregular coasts*. PhD thesis, McGill University, Montreal, Canada.

Forrer, H. and Jeltsch, R. 1998. A higher-order boundary treatment for Cartesian-grid methods. *J. Comput. Phys*. **140**, 259–277.

Gent, P. R. 1993. The energetically consistent shallow water equations. *J. Atmos. Sci*. **50**, 1323–1325.

Gent, P. R. and McWilliams, J. C. 1990. Isopycnal mixing in ocean circulation models. *J. Phys. Oceanogr*. **20**, 150–155.

Gerdes, R. 1993. A primitive equation ocean general circulation model using a general vertical coordinate transformation. *J. Geophys. Res*. **98**, 14683–14701.

Gill, A. E. 1982. *Atmosphere–ocean dynamics*, vol. 30 of *International Geophysics Series*. Academic Press, New York, 622 pp.

Hirst, A. and McDougall, T. J. 1996. Deep-water properties and surface buoyancy flux as simulated by a z-corrdinate model including eddy-induced advection. *J. Phys. Oceanogr*. **26**, 1320–1343.

Ierley, G. R. and Sheremet, V. A. 1995. Multiple solutions and advection-dominated flows in the wind-driven circulation. Part I: Slip. *J. Marine Res*. **53**, 703–738.

Killworth, P. D. and Edwards, N. R. 1999. A turbulent bottom boundary layer code for use in numerical ocean models. *J. Phys. Oceanogr*. **29**, 1221–1238.

Lohmann, G. 1998. The influence of a near-bottom transport parameterization on the sensitivity of the thermohaline circulation. *J. Phys. Oceanogr*. **28**, 2095–2103.

Madec, G. Chartier, M., Delecluse, P. and Crepon, M. 1991. A three-dimensional study of deep-water formation in the northwestern mediterranean sea. *J. Phys. Oceanogr*. **21**, 1349–1371.

Matthews, K., Noye, J. and Bills, P. 1996. A new method for numerical representation of the land-water boundary in lake circulation models. *Appl. Math. Modelling* **20**, 562–571.

Pedersen, G. 1986. On the effect of irregular boundaries in finite difference models. *Int. J. Num. Methods in Fluids* **6**, 497–505.

Pedlosky, J. 1996. *Ocean circulation theory*. Springer-Verlag, Heidelberg, 453 pp.

Pedlosky, J. 1987. *Geophysical fluid dynamics*. 2nd edn., Springer-Verlag, New York, 710 pp.

Pember, R., Bell, J., Colella, P., Crutchfield, W. and Welcome, M. 1995. An adaptive cartesian grid method for unsteady compressible flow in irregular regions. *J. Comput. Phys*. **120**, 278–304.

Phillips, A. N. 1957. A coordinate system having some special advantages for numerical forecasting. *J. Meteorol*. **14**, 184–185.

Roberts, M. J., Marsh, R., New, A. L. and Wood, R. A. 1996. An intercomparison of a Bryan-Cox-type ocean model and an isopycnic ocean model. Part I: The subpolar gyre and high latitude processes. *J. Phys. Oceanogr*. **26**, 1495–1527.

Roberts, M. J. and Wood, R. A. 1997. Topographic sensitivity studies with a Bryan–Cox type ocean model. *J. Phys. Oceanogr*. **27**, 823–836.

Sadourny, R. 1975. The dynamics of finite difference models of the shallow water equations. *J. Atmos. Sci*. **32**, 680–689.

Schwab, D. J. and Beletsky, D. 1998. Propagation of Kelvin waves along irregular coastlines in finite-difference models. *Adv. Water Resources* **22**, 239–235.

Shchepetkin, A. F. and O'Brien, J. 1996. A physically consistent formulation of lateral friction in shallow-water equation ocean models. *Mon. Weather Rev*. **124**, 1285–1300.

Wells, N. C. and de Cuevas, B. A. 1995. Depth-integrated vorticity budget of the southern ocean from a general circulation model. *J. Phys. Oceanogr*. **25**, 2569–2582.

Winton, M., Hallberg, R. and Gnanadesikan, A. 1998. Simulation of density-driven frictional downslope flow in z-coordinate ocean models. *J. Phys. Oceanogr*. **27**, 2163–2174.